PROCEEDINGS OF SCIENCE

Machine-learning aided detector optimization of the Pacific Ocean Neutrino Experiment

Christian Haack[a,*] **and Lisa Schumacher**[a] **for the P-ONE Collaboration**

[a] *Erlangen Centre for Astroparticle Physics, FAU Erlangen*
Nikolaus-Fiebiger-Straße 2, Erlangen, Germany

E-mail: christian.haack@fau.de, lisa.schumacher@fau.de

The Pacific Ocean Neutrino Experiment (P-ONE) is a planned cubic-kilometer-scale neutrino detector in the Pacific Ocean. P-ONE will measure high-energy astrophysical neutrinos to characterize the nature of astrophysical accelerators. Using existing deep-sea infrastructure provided by Ocean Networks Canada (ONC), P-ONE will instrument the ocean with optical modules - which host PMTs and readout electronics - deployed on several vertical cables of about 1 km in length. While the hardware design of the first prototype cable is currently being finalized, the detector geometry of the final instrument (up to 70 cables) is not yet fixed. Conventional design optimization typically requires extensive Monte-Carlo simulations, which limits the testable search space to a few configurations. In this contribution, we present the progress of optimizing the detector design using machine-learning-based surrogate models, which replace the computationally expensive MC simulations. By providing gradients, these models also allow for the efficient computation of detector resolutions via the Fisher Information Matrix, without having to rely on specific event-reconstruction algorithms. We present the physics sensitivities of various possible detector geometries calculated with the PLEnuM software tool.

38th International Cosmic Ray Conference (ICRC2023)
26 July - 3 August, 2023
Nagoya, Japan

*Speaker

PoS(ICRC2023)1059

1. Introduction

The Pacific Ocean Neutrino Experiment (P-ONE) is a planned multi-cubic-kilometer neutrino telescope in the Pacific Ocean [1]. P-ONE will be deployed at Cascadia basin, off the coast of Vancouver Island. There, it will be integrated into the already existing NEPTUNE observatory, hosted by Ocean Networks Canada (ONC). NEPTUNE consists of a 800 km-long cable loop, providing power and optical communication, with several access nodes along the loop. P-ONE will instrument the ocean with an array of optical modules (POMs). The POMs are deployed on cables that are moored to the seabed. Each POM houses 16 photo-multiplier tubes (PMTs), together with high-voltage power supply, digitization, and communication electronics. The first prototype detector line (P-ONE-1) is currently under construction [2]. On a length of just above 1 km, it will support 20 POMs with 50 m vertical spacing. P-ONE-1 is designed to be the first line of a full detector array targeting 70 lines.

Similar to existing neutrino telescopes, such as IceCube, KM3NeT, and Baikal-GVD, P-ONE will detect neutrinos by measuring Cherenkov light from secondary particles produced in neutrino interactions. The properties of the final state of the neutrino interaction, such as the energies and momenta of the secondary particles, determine the observable data. Different neutrino flavors and interaction types result in different event morphologies. In water or ice, hadronic and electromagnetic (EM) particle cascades produced in neutrino interactions typically evolve over a distance of 10 m to 20 m, hence resulting in a localized light emission compared to the POM spacing. ν_μ CC interactions produce secondary muons, which are able to propagate for large distances, resulting in long tracks of light emission. ν_τ CC interactions can result in a variety of complex morphologies and are not discussed further in this work.

Track-type and cascade-type morphologies are complementary in terms of detection efficiency and reconstruction resolutions. Due to their large "lever arm" (photons are emitted over a large distance), tracks typically have a good angular resolution. However, high-energy muons can propagate for several kilometers in ice or water, hence no calorimetric energy measurement is possible. This results in poor energy resolution. Cascades are complementary as their lever arm is significantly shorter, such that the light emission is contained in the detection volume. This results in a poorer angular resolution, but a calorimetric energy measurement is possible. As a result, the different event morphologies have different scaling behavior in terms of detection efficiency and resolution depending on the detector design: cascades benefit primarily from a densely instrumented detector, whereas tracks benefit from a larger lever arm.

The properties of the different event topologies make the optimization of the detector geometry of the full 70-string detector a non-trivial exercise. In the following, we will present a machine-learning-aided pipeline for optimizing the detector design. This allows us to efficiently obtain figures of merit for a wide range of possible detector designs, which is complementary to the conventional simulation-based approach presented in [3, 4].

2. Detector Response

The detector response for a given detector geometry is calculated as a function of the properties of incoming neutrinos in order to optimize the detector geometry of P-ONE. The relevant neutrino

properties are: Energy E, direction $\Omega = \{\theta, \phi\}$, flavor f and interaction vertex position $\vec{x}$.

The detector response consists of two parts: The first is the probability of detecting a neutrino with properties $(E, \Omega, f, \vec{x})$. This probability is typically characterized by the effective area[1], which relates the differential, per flavor neutrino flux $d\Phi_{\nu_f}/dEd\Omega$ at Earth's surface and the neutrino detection rate R_f:

$$R_f = \int \frac{d\Phi_{\nu_f}}{dEd\Omega} A^f_{\text{eff}}(E, \Omega) \cdot T_f(E, \Omega, \vec{x}) \cdot I_f(E, \Omega, \vec{x})\ dE\ d\Omega. \tag{1}$$

Here, T_f is the transmission probability of a neutrino of flavor f from Earth's surface to the detector and I_f is the interaction probability in (or near) the detector. We define the effective area as:

$$A^f_{\text{eff}}(E, \Omega, \vec{x}) = A_{\text{geo}} \cdot \epsilon_f(E, \Omega, \vec{x}), \tag{2}$$

where A_{geo} is the geometric area of the detector and ϵ is the detection efficiency. T and I can be obtained analytically, whereas ϵ is typically obtained from Monte-Carlo simulations. Especially for cascades, another useful quantity for studying the detection efficiency is the effective Volume:

$$V_{\text{eff}} = V_{\text{geo}} \cdot \epsilon_f(E, \Omega, \vec{x}), \tag{3}$$

where V_{geo} is the instrumented volume.

The second part of the detector response is the detector resolution. The neutrino interaction, light yield, and detection process are all stochastic processes, hence we need to obtain estimators (reconstructions) of the neutrino properties by statistical inference. Formally, the detector resolution is the conditional probability density: $p(\hat{E}, \hat{\Omega}, \hat{\vec{x}} \mid E, \Omega, \vec{x})$, where $\hat{E}, \hat{\Omega}, \hat{\vec{x}}$ are the reconstructed quantities. Written in this fashion, this function can also be interpreted as the likelihood of the reconstructed quantities for given true quantities. While this function contains the full information about the resolution, it is often useful to calculate a summary statistic to compare different detector configurations. Here, we use the covariance: $\xi = \text{cov}[(p(\hat{E}, \hat{\Omega}, \hat{\vec{x}}) \mid E, \Omega, \vec{x}]$.

3. Surrogate Model

Calculating the detection efficiency, ϵ, and the detector response, ξ, typically requires large-scale Monte-Carlo simulations. These simulations are made for a fixed detector geometry, and an update to the geometry requires a new simulation. Here, we propose to use a surrogate model, which allows us to parametrize large parts of the MC simulation pipeline and thus calculate ϵ and ξ at a fraction of the computational cost of a conventional simulation campaign.

Neutrino telescopes measure the arrival time, t_{ij}, per photon j and the total number of photons, n_i, at each PMT i. Their distributions contain all observable information from neutrino interactions inside the detector. Hence, we build a surrogate model which predicts the arrival time distribution and expected photon counts at each PMT as a function of the final state parameters of a neutrino interaction. Once these distributions are calculated, the response of the PMTs, the digitization and respective uncertainties can be obtained subsequently; this is not yet included in this work.

[1]The product of effective area, transmission and interaction probability is often referred to as "neutrino effective area", whereas the effective area as defined here is also referred to as "muon effective area".

For the surrogate model, we assume a single POM as base detection unit. As the data measured by each POM are independent[2], it is sufficient to construct a surrogate model for a single POM. Assuming that the detector medium is homogeneous, we evaluate the neutrino final state position and direction in a coordinate system relative to the POM.

Our surrogate model consists of two parts: The first predicts the arrival time distribution and the second predicts the expected amplitude. The arrival time distribution is modeled using a rational quadratic (RQ) normalizing flow [5, 6]. A normalizing flow transforms samples X drawn from a base distribution, $p_X(x)$, to a target distribution, $p_Y(y)$, using an invertible function $y = f_\theta(x)$. The PDF, $p_Y^\theta(y)$, of the transformed variable Y is obtained through the change of variables formula for random variables

$$p_Y^\theta(y) = p_X(f_\theta^{-1}(y)) \cdot \left| \frac{df^{-1}}{dy} \right|. \tag{4}$$

This construction allows both drawing a sample from the target distribution and evaluating the PDF. For RQ normalizing flows, the function f is chosen as a k piecewise, monotonic rational quadratic splines. The flow is parametrized by $3k - 1$ parameters θ, which determine the spline knots and their derivatives. Manipulating θ allows the flow to transform the base distribution into a wide range of shapes. Here, our target distribution $p_Y^\theta(y)$ is the photon arrival time distribution. We obtain samples y_i with our simulation pipeline and use maximum likelihood estimation to obtain the flow parameters θ.

To encode the change of the arrival time distribution as a function of the neutrino final state parameters $\vec{u} = (E, \theta, \phi, \ldots)$, we use a neural network (multi-layer perceptron, MLP) to predict the flow parameters θ: Hence, our optimization procedure now consists of optimizing the MLP parameters (using stochastic gradient descent), with loss function $-\mathcal{L}(y_i, \theta)$. Evaluating the arrival time distribution for a given parameter vector $\vec{u}$ now consists of first obtaining the encoded normalizing flow parameters $\theta(\vec{u})$ from the neural network and then evaluating Equation 4.

The prediction of the expected amplitude λ is done with a second MLP, which is trained to predict $\log \lambda$ using a Poisson loss. Using both models, we construct the likelihood of observing n_i photons at times t_{ij} at a PMT i:

$$\mathcal{L}_i(\{t_{ij}\}, n_i \mid \vec{u}) = \exp(-\lambda(\vec{u})) \cdot \frac{\lambda(\vec{u})^k}{k!} \cdot \prod_j^{n_i} \cdot p^{\theta(\vec{u})}(t_{ij}). \tag{5}$$

Using this likelihood, we calculate the Fisher Information Matrix:

$$I_{ij}(\vec{u}) = E\left[\frac{\partial \log \mathcal{L}}{\partial \theta_i} \cdot \frac{\partial \log \mathcal{L}}{\partial \theta_j} \middle| \vec{u} \right], \tag{6}$$

where the expectation value is evaluated by drawing samples from the underlying probability density functions. The partial derivatives are evaluated using automatic differentiation. Finally, the Cramér-Rao bound states that the covariance of any unbiased estimator $T(\{t_{ij}\}, n_i)$ of the parameters $\vec{u}$ is bounded by:

$$\mathrm{cov}(T(\vec{u})) \geq I^{-1}(\vec{u}). \tag{7}$$

[2]Module shadowing can be neglected

Hence, the inverse Fisher Information Matrix allows us to calculate the statistical limit of the detector resolution achievable with a certain detector configuration.

4. Detector Simulation

The training data for the surrogate model is obtained from a conventional detector simulation. In general, these simulations consist of the following steps: 1) Simulation of the neutrino interaction and computation of the final states. 2) Evolution/propagation of the final states and calculation of the Cherenkov light yield. 3) Propagation of Cherenkov photons to detection modules / PMTs. 4) Calculation of the PMT response and readout. 5) Trigger simulation. For the purposes of neutrino telescopes, the total Cherenkov light yield of high-energy hadronic and EM particle cascades can be parametrized in order to avoid expensive MC evolution of the full particle cascade [7].

Additionally, most event topologies can be approximated by a combination of hadronic (or EM) particle cascades and muons. For this study, we average the stochastic energy losses of energy muons, resulting in "lightsaber" muons. Lightsaber muons of energy E emit a constant number of photons per length, where this constant is derived from the mean light yield of stochastic muons.

High-energy neutrino interactions can produce upwards of 10^{10} photons. Exact simulation of the resulting photon trajectories, including scattering in the medium, is computationally expensive. Here, we use a custom GPU-based photon propagation code[3] to obtain the training data for the surrogate model, i.e. photon arrival time distributions and expected number of hits. We assume the detection medium (ocean water) to be homogeneous, with optical properties as measured by the STRAW experiment [8]. We produce two simulation sets to train the surrogate model: One for lightsaber muons and one for EM cascades. These allow us to quantify the detector response of the most important event classes.

5. Results

Figure 1 shows a comparison between the full MC photon propagation and the surrogate model expectation for lightsaber muons for the total number of detected photons summed over all PMTs. The surrogate model accurately captures the distance dependence of the expected photon flux. Models trained on different subsets of the training data allow quantifying the model uncertainty.

We use the surrogate models to study a toy P-ONE detector with 70 detector lines. Each line is modeled after P-ONE-1, thus containing 20 POMs with 50 m vertical spacing. The lines are arranged in clusters of 10 lines each, where 6 clusters are arranged radially around the central 7th cluster. The lines in each cluster are arranged on a hexagonal grid. We use a scaling parameter ("spacing") to scale the hexagonal grid of each cluster, as well as the distance between clusters. For all studies, we keep the total number of sensors fixed, so that the spacing effectively controls the sensor density. The detection efficiency is obtained by evaluating the amplitude surrogate model. P-ONE will use a triggered data readout, which at its core will consist of a module-level local-coincidence trigger (LC), requiring $\geq n_{LC}$ hits on two separate PMTs per POM. A simple event trigger then consists of requiring $\geq n_{POM}$ fulfilling the LC condition. Since we do not consider noise in this study, we also do not include any time-based information in our trigger definitions. In

[3] https://github.com/PLEnuM-group/PhotonPropagation.jl

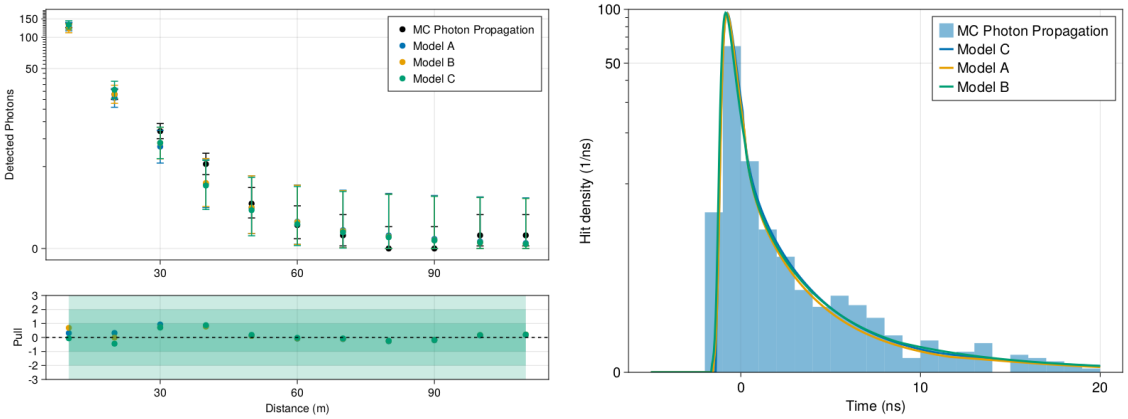

(a) Detector number of photons as function of the closest approach distance to the POM.

(b) Time residual distribution of a single PMT for a distance of 6 m to the muon track.

Figure 1: MC photon propagation for a lightsaber muon with $E = 50$ TeV compared to the surrogate model predictions. Models A, B, and C are surrogate models trained on different subsets of the full training sample.

the following, we choose $n_{LC} = 2$ and $n_{POM} = 3$. The resulting detection efficiency is shown in Figure 2. The optimal spacing for both tracks and cascades is strongly energy dependent, although comparable for both morphologies. For the highest energies, the effective area/volume surpasses the instrumented volume. This is due to uncontained events which pass outside the instrumented volume, but deposit enough light in the outer POMs to fulfill the trigger condition.

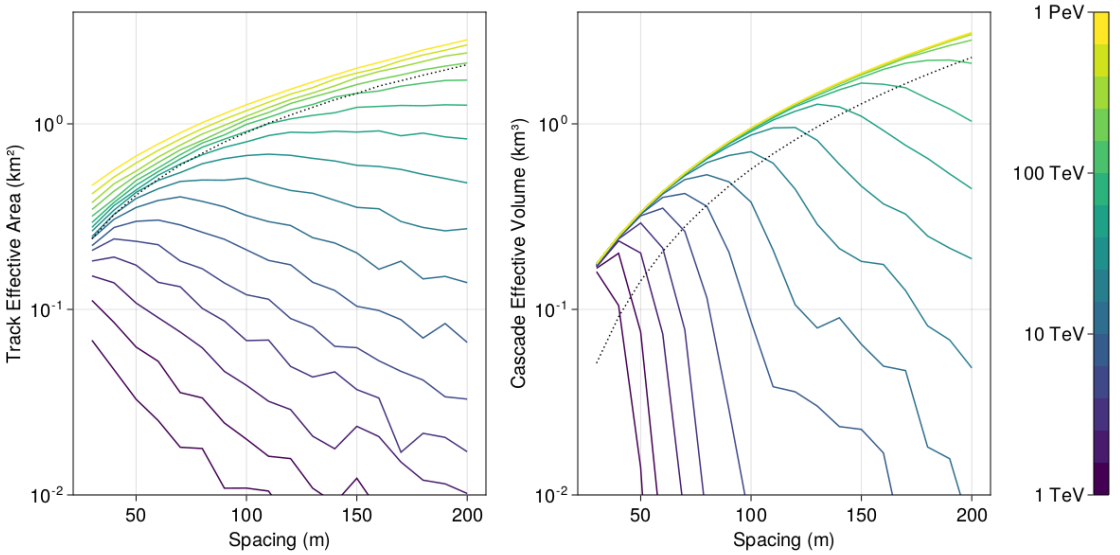

Figure 2: Predicted muon effective area for lightsaber muons (left) and effective volumes for cascades (right) using the surrogate model. The dotted lines show the geometric area and the geometric volume of the detector. For the area, it is averaged over a uniform direction of tracks.

Figure 3 shows the angular resolutions derived from the Cramér-Rao covariance matrix. For Cascades, the resolution monotonically degrades as a function of the string spacing. For horizontal

tracks (between 70 deg and 110 deg zenith angle) the increasing lever arm can compensate for the decrease in sensor density, with an optimum visible at medium energies at $\approx$ 80 m. For vertical tracks, the resolution degrades quickly with increasing spacing.

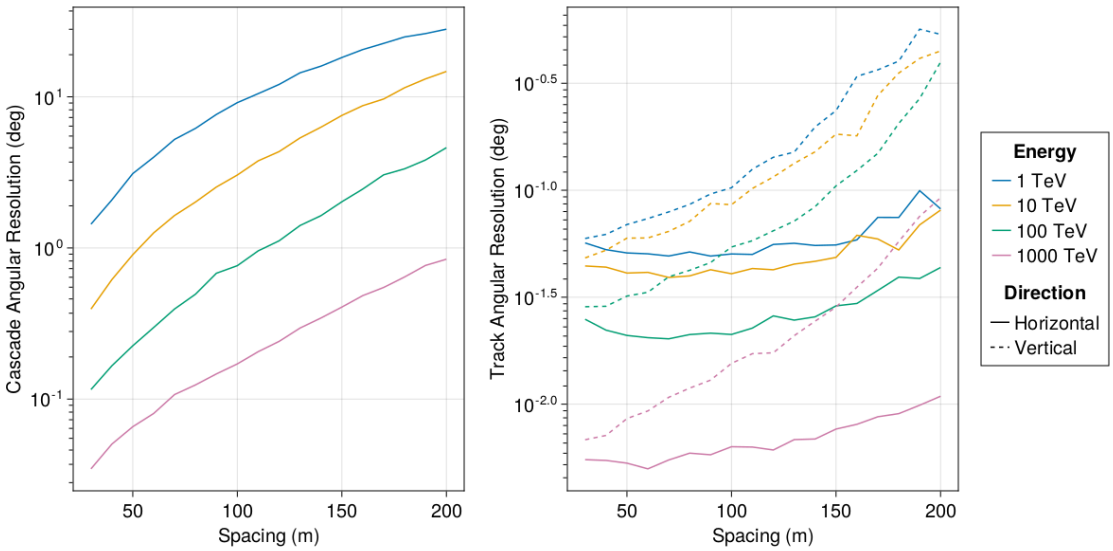

Figure 3: Predicted angular resolution for cascades and lightsaber muons and using the surrogate model and the Cramér-Rao averaged over a uniform flux.

The predicted detector response allows us to conduct a toy sensitivity study for a typical benchmark analysis in neutrino telescopes. We use nuSQuIDS[4] to propagate neutrinos through Earth and the CSMS [9] cross-section to calculate the neutrino interaction probability for $\nu_e - CC$ interactions. The resulting neutrino effective areas and resolutions are used in the PLEnuM-tool[10] to calculate the expected discovery potential for measuring the isotropic astrophysical neutrino flux with 10 years of livetime[5]. The resulting significance as a function of the line spacing is shown in Figure 4.

6. Conclusions

In this contribution, we present a novel method for optimizing the detector geometry of a neutrino telescope. A surrogate model based on normalizing flows can learn the detector response, giving access to the full detector likelihood function. This does not only enable efficient event simulations for arbitrary detector configurations but also the calculation of the statistical limit of the detector resolution achievable for a given detector geometry. Using the planned P-ONE neutrino telescope as a motivation, we have demonstrated how the surrogate model can be used to calculate the detector response as a function of the horizontal line spacing. In the future, the detector response can be fed into analysis frameworks (such as PLEnuM) to calculate figures of merit for a wide range of science cases as a function of the detector geometry.

[4]https://github.com/arguelles/nuSQuIDS
[5]Note, this includes only the $\nu_e - CC$ channel

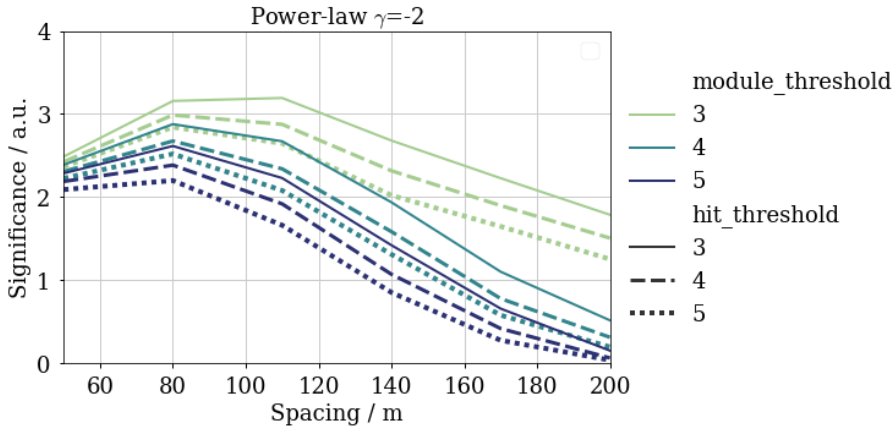

Figure 4: OLD PLOT: Discovery potential of the isotropic astrophysical flux in arbitrary time units using EM cascades

Acknowledgements

We thank Ocean Networks Canada for the very successful operation of the NEPTUNE observatory, as well as the support staff from our institutions without whom P-ONE could not be operated efficiently. We acknowledge the support of Natural Sciences and Engineering Research Council, Canada Foundation for Innovation, Digital Research Alliance, and the Canada First Research Excellence Fund through the Arthur B. McDonald Canadian Astroparticle Physics Research Institute, Canada; European Research Council (ERC), European Union; Deutsche Forschungsgemeinschaft (DFG), Germany; National Science Centre, Poland; U.S. National Science Foundation-Physics Division, USA.

References

[1] M. Agostini et al., *Nat Astron* **2020**, *4*, 913–915, DOI 10.1038/s41550-020-1182-4.

[2] C. Spannfellner, *PoS*, *ICRC2023*, 1219.

[3] F. Henningsen et al., *PoS*, *ICRC2023*, 1053.

[4] J. P. Twagirayezu et al., *PoS*, *ICRC2023*, 1175.

[5] I. Kobyzev et al., *IEEE PAMI* **2021**, *43*, 3964–3979, DOI 10.1109/TPAMI.2020.2992934.

[6] C. Durkan et al., Neural Spline Flows, **2019**, DOI 10.48550/arXiv.1906.04032.

[7] L. Rädel et al., *APh* **2013**, *44*, 102–113, DOI 10.1016/j.astropartphys.2013.01.015.

[8] N. Bailly et al., *EPJC* **2021**, *81*, 1071, DOI 10.1140/epjc/s10052-021-09872-5.

[9] A. Cooper-Sarkar et al., *JHEP* **2011**, *2011*, 42, DOI 10.1007/JHEP08(2011)042.

[10] L. J. Schumacher et al., *PoS* **2021**, *ICRC2021*, 1185, DOI 10.22323/1.395.1185.

Full Authors List: P-ONE Collaboration

Matteo Agostini[11], Nicolai Bailly[1], A.J. Baron[1], Jeannette Bedard[1], Chiara Bellenghi[2], Michael Böhmer[2], Cassandra Bosma[1], Dirk Brussow[1], Ken Clark[3], Beatrice Crudele[11], Matthias Danninger[4], Fabio De Leo[1], Nathan Deis[1], Tyce DeYoung[6], Martin Dinkel[2], Jeanne Garriz[6], Andreas Gärtner[5], Roman Gernhäuser[2], Dilraj Ghuman[4], Vincent Gousy-Leblanc[2], Darren Grant[6], Christian Haack[14], Robert Halliday[6], Patrick Hatch[3], Felix Henningsen[4], Kilian Holzapfel[2], Reyna Jenkyns[1], Tobias Kerscher[2], Shane Kerschtien[1], Konrad Kopański[15], Claudio Kopper[14], Carsten B. Krauss[5], Ian Kulin[1], Naoko Kurahashi[12], Paul C. W. Lai[11], Tim Lavallee[1], Klaus Leismüller[2], Sally Leys[8], Ruohan Li[2], Paweł Malecki[15], Thomas McElroy[5], Adam Maunder[5], Jan Michel[9], Santiago Miro Trejo[5], Caleb Miller[4], Nathan Molberg[5], Roger Moore[5], Hans Niederhausen[6], Wojciech Noga[15], Laszlo Papp[2], Nahee Park[3], Meghan Paulson[1], Benoît Pirenne[1], Tom Qiu[1], Elisa Resconi[2], Niklas Retza[2], Sergio Rico Agreda[1], Steven Robertson[5], Albert Ruskey[1], Lisa Schumacher[14], Stephen Sclafani[12 α], Christian Spannfellner[2], Jakub Stacho[4], Ignacio Taboada[13], Andrii Terliuk[2], Matt Tradewell[1], Michael Traxler[10], Chun Fai Tung[13], Jean Pierre Twagirayezu[6], Braeden Veenstra[5], Seann Wagner[1], Christopher Weaver[6], Nathan Whitehorn[6], Kinwah Wu[11], Juan Pablo Yañez[5], Shiqi Yu[6], Yingsong Zheng[1]

[1]Ocean Networks Canada, University of Victoria, Victoria, British Columbia, Canada.
[2]Department of Physics, School of Natural Sciences, Technical University of Munich, Garching, Germany.
[3]Department of Physics, Engineering Physics and Astronomy, Queen's University, Kingston, Ontario, Canada.
[4]Department of Physics, Simon Fraser University, Burnaby, British Columbia, Canada.
[5]Department of Physics, University of Alberta, Edmonton, Alberta, Canada.
[6]Department of Physics and Astronomy, Michigan State University, East Lansing, MI, USA.
[8]Department of Biological Sciences, University of Alberta, Edmonton, Alberta, Canada.
[10]Gesellschaft für Schwerionenforschung, Darmstadt, Germany.
[11] Department of Physics and Astronomy and Mullard Space Science Laboratory, University College London, United Kingdom
[12] Department of Physics, Drexel University, 3141 Chestnut Street, Philadelphia, PA 19104, USA.
[13] School of Physics and Center for Relativistic Astrophysics, Georgia Institute of Technology, Atlanta, GA, USA.
[14] Erlangen Centre for Astroparticle Physics, Friedrich-Alexander-Universität Erlangen-Nürnberg, D-91058 Erlangen, Germany.
[15] H. Niewodniczański Institute of Nuclear Physics, Polish Academy of Sciences, Radzikowskiego 152, 31-342 Kraków, Poland.
$^{\alpha}$ now at Department of Physics, University of Maryland, College Park, MD 20742, USA.

PoS(ICRC2023)1059